Laser-assisted surface activation for the fabrication of flexible non-enzymatic Cu-based sensors

Evgeniia M. Khairullina[1], Karolis Ratautas[2] , Maxim S. Panov[1], Vladimir S. Andriianov[1], Sarunas Mickus[2], Alina A. Manshina[1], Gediminas Račiukaitis[2], Ilya I. Tumkin[1]

[1]Saint Petersburg State University, 7/9 Universitetskaya nab., St. Petersburg 199034, Russia;
[2] Center for Physical Sciences and Technology, 231 Savanoriu ave., Vilnius 02300, Lithuania
*Correspondence: i.i.tumkin@spbu.ru (I.I.T.)

Keywords: selective surface activation induced by a laser; non-enzymatic sensors; glucose, hydrogen peroxide, dopamine

Abstract
We developed a rapid and effective technique for fabrication of sensor-active copper-based materials on the surface of such flexible polymers as terephthalate, polyethylene naphthalate and polyimide using the method of laser surface modification. For this purpose, we optimized the polymer surface activation parameters using laser sources with a picosecond pulse duration for subsequent selective metallization within the activated region. Further, the fabricated copper structures were modified with gold nanostructures and by electrochemical passivation to produce copper-gold and oxide-containing copper species, respectively. As a result, in comparison with pure copper electrodes, these composite materials exhibit much better electrocatalytic performance concerning the non-enzymatic identification of biologically important disease markers as glucose, hydrogen peroxide and dopamine.

Introduction

Traditional medical services require professional personnel and expensive equipment for conducting diagnostics based on the analysis of biological fluid markers, which imposes significant restrictions on the possibilities of long-term monitoring in real-time. However, these restrictions can be overcome using miniature wearable electronics and sensors. Furthermore, such portable devices can be used in environmental safety, the food industry and forensic medical examination.

At present, there are many methods for detecting biologically essential analytes (such as glucose, hydrogen peroxide, etc.), among which the most common are titrimetry, spectrophotometry, chemiluminescence, and electrochemical methods as the most effective and promising in this regard. Typically, the electrochemical approach involves the implementation of the enzymatic sensors, i.e. devices that include a bio-detecting agent (enzyme) immobilized on the surface of a working electrode, selectively binding to the target analyte. For example, in the case of glucose detection, glucose oxidase (GO_x) or glucose dehydrogenase are used, whereas lactose oxidase is used for lactate sensing. However, the enzyme-based sensors are characterized by many significant disadvantages associated with the use of enzyme molecules, which are sensitive to pH, high temperatures, humidity, and the presence of dissolved oxygen in the studied system [1]. On the other hand, there is a promising alternative – enzyme-free sensing. In this case, it is not necessary to use functional biological units. Non-enzymatic sensors are characterized by structural simplicity, which provides higher reproducibility and quality control for mass production and are free of the above-mentioned disadvantages of enzyme sensors. In addition, they have a higher sensitivity due to the direct electron transfer from the analyte molecule to the electrocatalytically

active center of an electrode without using a mediator or an enzyme [2, 3]. Thus, the development of flexible electrochemical sensor platforms without a bio-detecting element, the selectivity of which is achieved due to the highly developed porous nanostructured electrode surface, is quite important from scientific and technological points of view.

Currently, a search for the most ergonomic form factor of sensor platforms for various applications deserves special attention [4]. Moreover, the possibility of creating flexible wearable devices in the form of temporary tattoos [5, 6], mouthguards [7], contact lenses [8], bracelets [9–11], patches [12, 13], gloves [14, 15] has been shown. As substrates, the most commonly used are polymer materials such as polyethylene naphthalate (PEN), polyethylene terephthalate (PET), polyvinyl membranes (PVA), acrylic tape, polyimide (PI), polyester, etc. [16]. Among them, PI is widely used in the production of flexible sensor devices due to its high chemical and thermal resistance (up to 300 ºC) [17–20]. However, its natural yellow color limits the use of this polymer, where transparency of the substrate is required. On the other hand, in the visible range, the transmission of PEN and PET is about 85%. In addition, they are more resistant to bending deformation. The vast majority of studies in the field of wearable sensor platforms is aimed at detecting biologically significant analytes and monitoring human health [21]. In turn, the potential of such devices is much wider, in particular they can be used in the field of environmental safety, food industry and forensic medical examination [22, 23]. For example, to detect medicines whose turnover is regulated by the state, explosives and other toxic and dangerous compounds to ensure transport security, express analysis at the crime scene [24].

The most common methods of synthesis of the electrode materials that require a separate stage for template fabrication are screen printing [25, 26], roll printing (R2R – roll-to-roll) [27], lithographic methods, including soft lithography, photolithography, and electron beam evaporation. Among the additive approaches, we can distinguish inkjet printing [28–30], a group of methods of direct laser writing (DLW), selective laser sintering [31], laser deposition, etc. An alternative to the methods described above is the stamp-printing of electrodes (STE-stamp transfer electrodes). This method allows manufacturing electrochemical sensors on non-planar surfaces of a simple shape with a small curvature radius applicable to dopamine and ascorbic acid detection [32]. The main disadvantages of the aforementioned methods are the complexity of producing alloys and composites of a necessary composition [33]. In addition, the decisive factor of the functional properties of enzyme-free sensors is the morphology of their surface. A more developed surface provides a greater number of active centers per unit of geometric area. However, it is not easy to obtain deposits with such characteristics using the methods described above in many cases.

One of the significant advantages of additive technologies is creating patterns of almost any given geometry, which is often unavailable for subtractive methods. Additive methods of direct laser deposition allow to fabricate a wide range of materials of different nature (metals, oxides, etc.) on the surface of different types, which can serve as electrodes for enzymeless sensing. The first group of such methods includes such techniques as laser-induced forward metal transfer (LIFT) and laser-induced metal deposition from solution (LCLD). For example, in LCLD, a localized effect on the metallization solution occurs, leading to decomposition of the metal precursor in the microreactor at the focus of the laser beam and reduction to the metallic state. As a result, it is possible to create metal patterns of any geometry by scanning the laser beam along the substrate surface [34, 35]. This method is a promising approach for the fabrication of non-enzymatic sensors with high electrocatalytic activity toward D-glucose, hydrogen peroxide and L-alanine detection [36]. However, a low deposition rate is one of the most serious disadvantages of

this method, which equals to about tens of microns per second. The second group of additive methods, e.g. laser direct structuring (LDS), deals with two-stage procedures, where the stages of the substrate activation and metallization are separated in time. Moreover, LDS is based on special metalorganic additives premixed in the polymeric substrate, thus limiting the application areas. In this work, we proposed a methodology based on such an approach. In our case, it is not required to use unique composites as substrates, and the metal reduction from solution occurs due to activation of the catalytic activity of the polymer surface by laser irradiation or due to implementation of a separate activator substance (as a rule, precious metal salts). Basically, in the case of polymer surfaces, the possibility of direct activation of the surface upon laser irradiation was shown for polyimide (PI) [37]. However, this process is kinetically inhibited (the growth of the conductive structures takes about five hours). The use of organometallic molecules (e.g. $Pd(AcAc)_2$), which are deposited on the polymer surface before irradiation and are decomposed under the action of a laser beam, makes it possible to selectively activate the surface of polyphenyl-quinoxaline and PET [38, 39].

This work contributes to the further development of the Selective Surface Induced by Laser (SSAIL) technique [40–43]. Furthermore, the proposed approach provides conditions for metallization of the surface of different polymers, avoiding the use of expensive and toxic organometallic molecules in favour of less expensive silver salts and allowing fabricating metallic and bimetallic structures based on the use of expensive silver salts of copper and gold with good electrocatalytic performance. Moreover, the modification of the electrode surface with such catalytically active and stable metal as gold exhibits many benefits. Indeed, there are extensive investigation of synergetic effect of different kind of materials in one composite system [44, 45]. This phenomenon may lead to faster electron transfer or other processes increasing electrochemical performance. Bimetallic Cu-Au alloys and composites reveal remarkable electrocatalytic activity with comparison to pure gold/copper materials [46–49]. The combination of precious (Au) and earthabundant (Cu) metals can lead to increasing of copper stability and it resistivity to oxidation, which supposed to improve shelf life of the sensor and reproducibility of the analysis. The gold was precious metal of choice due to high stability compared to silver nanomaterials and relatively low price with respect to Pd, Pt, ect.

Materials and methods

Laser activation and metallization of the polymer surface

All sensor-active materials were fabricated using laser activation of polymeric surfaces with subsequent selective metallization. This approach includes four stages: (1) laser modification of the polymer surface in the air; (2) treatment of the substrate with silver nitrate solution; (3) copper plating of the activated region; (4) modification of the fabricated copper structures to increase the electrocatalytic activity toward the target analyte. Polyethylene terephthalate (PET), polyethylene naphthalate (PEN) and polyimide (PI) were obtained in Sigma Aldrich and were used as substrates. Substrates were cleaned in an ultrasonic bath with water/alcohol/acetone mixture for 15 min before synthesis and dried in the air. Ultrapure water (18.2 MΩ·cm) was used for preparation of all the aqueous solutions.

In the first stage (1), laser modification of polymers was carried out using the focused (the diameter of the focal spot was 25 μm) laser irradiation with a wavelength of 532 nm, a pulse length of 10 ps, a pulse repetition rate of 5-200 kHz and an average power of up to 15 W. A pulse picker was used to vary the pulse repetition rate and a lens with a focal length of 160 mm was used to focus the laser beam on the polymer surface. The optimal fabrication parameters of copper

electrodes for each substrate are presented in the results and discussion section. The laser beam was moved relative to the substrate using a galvanometric scanner (Scanlab AG). The chemical activation associated with stage (2) was performed by holding the irradiated substrate in a solution of 5×10^{-4} M silver nitrate for 8 minutes at room temperature, after which the sample was thoroughly washed with a large amount of distilled water to remove silver ions from the non-irradiated surface of a polymer. Next, the selective chemical deposition of copper on the activated polymer surface was done in stage (3). In this regard, the substrate was placed for 30 minutes at 30°C in an aqueous solution for metallization (Fig. 1). The composition of this solution can be found in Table S1. The reduction reaction of copper ions with formaldehyde proceeded according to Scheme S1. This process is autocatalytic. After forming the first copper crystals due to the activation of the surface at the previous stages of synthesis, further growth of the deposit is catalyzed by the forming metallic copper. All chemical reagents used in this work had a degree of purity not lower than analytical grade and were commercially available (Sigma Aldrich).

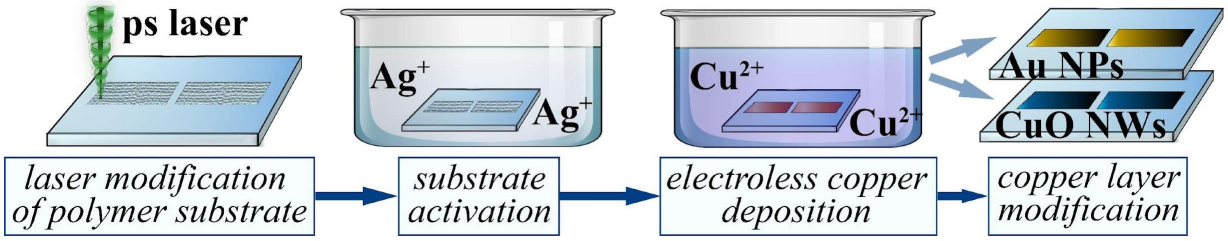

Fig. 1 Stages of laser-assisted fabrication of flexible non-enzymatic Cu-based sensors.

Modification of the surface of copper electrodes

To improve the analytical characteristics of the fabricated copper electrodes, we performed their modification with gold. The procedure was based on Ref. [50]. The modification of the synthesis described in [50] was made to localize the chemical reaction of gold ions reduction. For this purpose, formaldehyde was excluded from the solution and copper layer itself was used as reducing agent. Gold nanostructures were synthesized on the electrode surface by reducing gold from an aqueous solution of hydrogen tetrachloraurate (0.007 M $HAuCl_4$) and 4-dimethylaminopyridine (0.1 M DMAP) with metallic copper at 60 °C for 5 minutes. Finally, the modified copper electrode was washed with a large amount of water and dried in the air.

Moreover, we produced oxide nanostructures on the surface of copper electrode using electrochemical passivation [51–53]. This synthesis was carried out in a standard three-electrode cell. The fabricated copper structures and platinum wire were used as working and counter electrodes, respectively, whereas, Ag/AgCl electrode was used as a reference. Passivation was performed for 600 seconds at a -200 mV (vs Ag/AgCl) potential in a background solution of 1 M NaOH. Upon these conditions, various oxidation processes of copper electrode may occur, which lead to the formation of such products as copper(I) oxide, copper(II) oxide and copper hydroxide. After passivation procedure, the fabricated nanowires were annealed in air atmosphere at 130 °C for 60 min to form CuO nanostructures [54].

Bending test

Bending test was performed by fixing the specimen on mechanical clamps connected through thread driven linear stage as shown in Fig. S1a. The dimensions of the copper trace were 70 x 3 mm. The thickness of the copper layer was ~1.5µm. The bending procedure was performed by changing the distance between the clamps to reach the minimum bending radius “R” (the minimum radius was chosen as 1 mm). The distance between claps was moved from 65 mm (when a specimen is flat) to 10 mm (when a specimen is highly bent) by “dx” = 55 mm (Fig. S1b). The

single bending cycle took 0.5 s. Resistance was in-situ observed during the test using the "Keithley 2610 B" multimeter device.

Morphology, analysis of atomic and phase composition

Morphology and composition of the obtained materials were studied using scanning electron microscopy (SEM), X-ray photoelectron spectroscopy (XPS) and energy dispersion of X-ray spectroscopy (EDX), respectively. The EDX-system was coupled with a Zeiss Supra 40 VP scanning electron microscope equipped with X-ray attachment (SEM, Zeiss Supra 40VP; EDX, INCA X-act, Oxford Instruments, UK). XPS analysis was performed using the photoelectron spectrometer "Escalab 250Xi" with AlKα radiation. Spectra were collected in the constant pass energy mode at 50 eV for element core level spectrum and 100 eV for survey spectrum (spot size 650 μm). In addition, the phase composition of copper-based electrodes was investigated by a Bruker D2 Phaser diffractometer equipped with a LynxEye detector (Bruker-AXS, Karlsruhe, Germany).

Electrochemical studies

Electrocatalytic activity of the fabricated electrode materials toward enzyme-free detection of D-glucose (Gl), hydrogen peroxide (H_2O_2) and dopamine (DA) was investigated using voltammetric methods at room temperature in a standard three-electrode cell mentioned before. Amperograms (CA) and cyclic (CV) voltammograms were recorded using Corrtest CS300 potentiostat (Wuhan Corrtest Instruments Ltd., China). Electrochemical testing of DA and H_2O_2 were conducted with 0.1 M PBS as background electrolyte, in turn 0.1 M NaOH was used in case of GL. All potentials mentioned in this work are referenced to Ag/AgCl electrode. CV experiments were performed at 50 mV/s scan rate for all electrodes, CA measurements for glucose, hydrogen peroxide and dopamine detection were carried out at 0.5 V, −0.17 V, and 0.25 V (vs. Ag/AgCl) respectively. Fabricated Cu-Au bimetallic electrodes were used for glucose detection in the blood serum samples. Serum samples were centrifuged, stored at 4°C, and injected into 0.1 M NaOH background solution before chronoamperometric analysis at potential 0.5 V (vs. Ag/AgCl). As reference, data measured with a portable commercial analyzer was used.

Results and discussion

Laser activation of the polymer surface with subsequent copper plating

As it was previously discussed, the synthesis of copper structures on the surface of polymers proceeded via three main stages: selective modification of the polymer by exposure in the field of laser radiation, activation of the polymer surface by holding it in $AgNO_3$ solution and chemical deposition of copper within the activated area. In this work, the main attention was paid to the first stage of the synthesis, i.e. the interaction of laser radiation with the polymer surface. At the same time, the most important physical parameters affecting two other stages (activation and chemical reduction of copper) are laser power, pulse repetition rate, scanning speed, and distance between producing copper lines. Parameters used for laser picosecond modification of the surface of used in the current work polymers: scanning speed, 2-6 m $s^{-1}$and distance between lines (*h*), 10-20 μm.

Fig. 2 and Figs S2-S3 demonstrate SEM images of the polymer surface under different laser exposure conditions and the corresponding result of chemical copper plating. The optimal conditions for laser modification were chosen based on the electrical resistance of the formed deposits, adhesion according to scotch tests, as well as a qualitative evaluation of the morphology of these deposits according to optical microscopy.

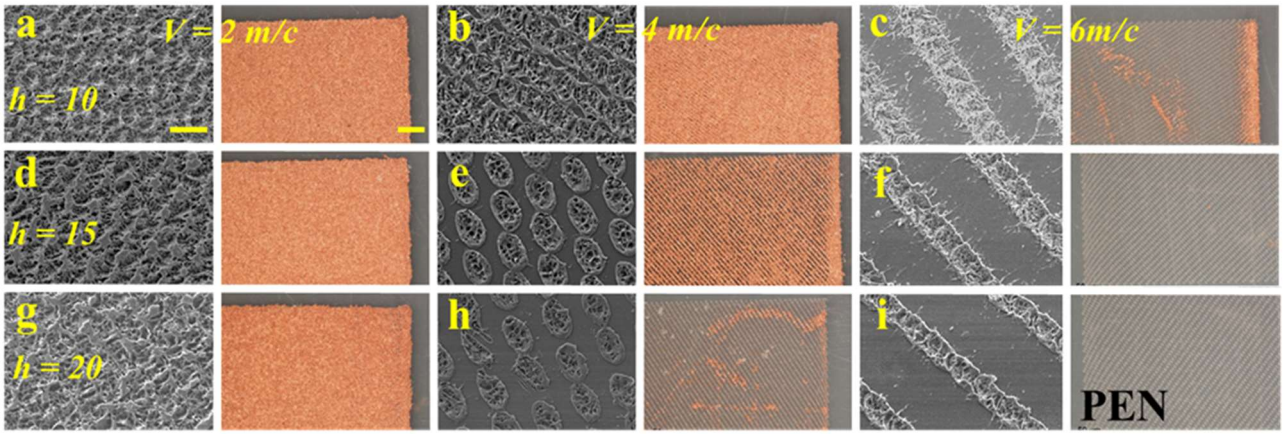

Fig. 2 Optical micrographs and SEM images of copper structures deposited on PEN using laser modification at different scanning speeds and distances between lines. (a) v=2 m s^{-1}, h=10, (b) v=4 m s^{-1}, h=10, (c) v=6 m s^{-1}, h=10, (d) v=2 m s^{-1}, h=15, (e) v=4 m s^{-1}, h=15, (e) v=6 m s^{-1}, h=15, (f) v=2 m s^{-1}, h=20, (h) v=4 m s^{-1}, h=20, (i) v=6 m s^{-1}, h=20. The size scale corresponds to 20 μm for SEM images and 500 μm for optical microphotographs.

As a result, the optimal synthetic conditions for all polymer substrates are demonstrated in Table 1, whereas optical photographs of the corresponding copper-based structures obtained at these conditions are shown in Fig. 3a.

Table 1 Optimal regimes for laser modification of the polymer surfaces.

Polymer	Laser power, W	Repetition rate, kHz	Scanning speed, m s^{-1}	h, μm
PI	3.000	100	4	15
PEN	0.983	100	2	10
PET	4.630	100	2	20

Depending on the nature of the substrate material, the interaction of laser radiation with the surface can lead to the initiation of various processes forming active centers that facilitate electron transfer in the redox reaction. In the case of polymers, a decrease in oxygen in the surface layer is observed. It may indicate the formation of new functional groups, e.g. the breaking of carbonyl and ether bonds as well as the formation of aldehydes, which can reduce silver from $AgNO_3$ solution at the surface activation stage [16]. However, in contrast to solid oxide materials, one can observe a significant local change in morphology and formation of a spongy structure with a developed surface that significantly increases the adhesion of the synthesized copper layers. Thus, it is possible to distinguish two mechanisms of modification of the polymer surface under the action of laser radiation concerning the local process of copper plating: change in either the nature or morphology of the surface layer.

The electrode for the bending test was fabricated using SSAIL method on 150 μm PET film, 1000 bending cycles were performed for the specimen. A slight increase in the resistance of the electrode during the bending test was observed. At the end of the cycle resistance value turned into saturation. The total increase of the resistance after the 1000 cycles was by 13.8 percent of the primary value (Fig. 3b).

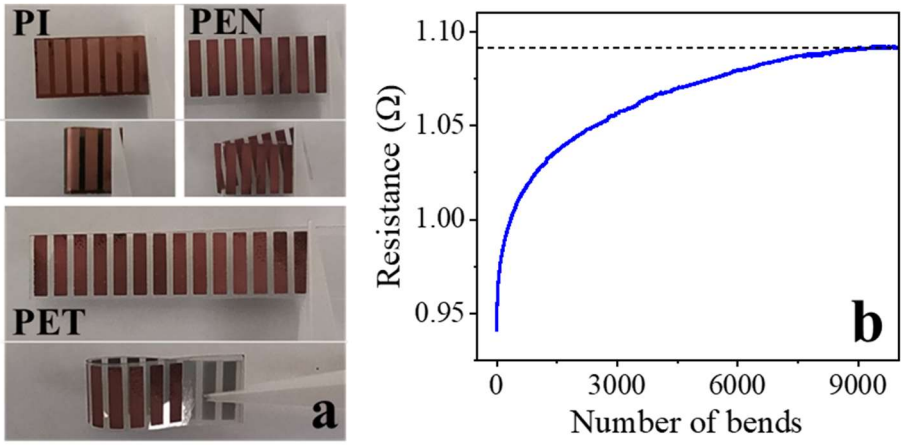

Fig. 3 (a) Photographs of copper structures on various polymers produced under optimal synthesis conditions; (b) bending test of PET plated electrode: resistance dependence on the number of bending.

The fabricated copper structures were examined using scanning electron microscopy and X-ray phase analysis (Fig. 4). According to these studies, all materials consist of pure metallic copper. The observed structures are solid films, which should provide a stable electrical contact during electrochemical studies. It can also be noted that copper deposits inherit the morphology of the substrate exposed to laser radiation.

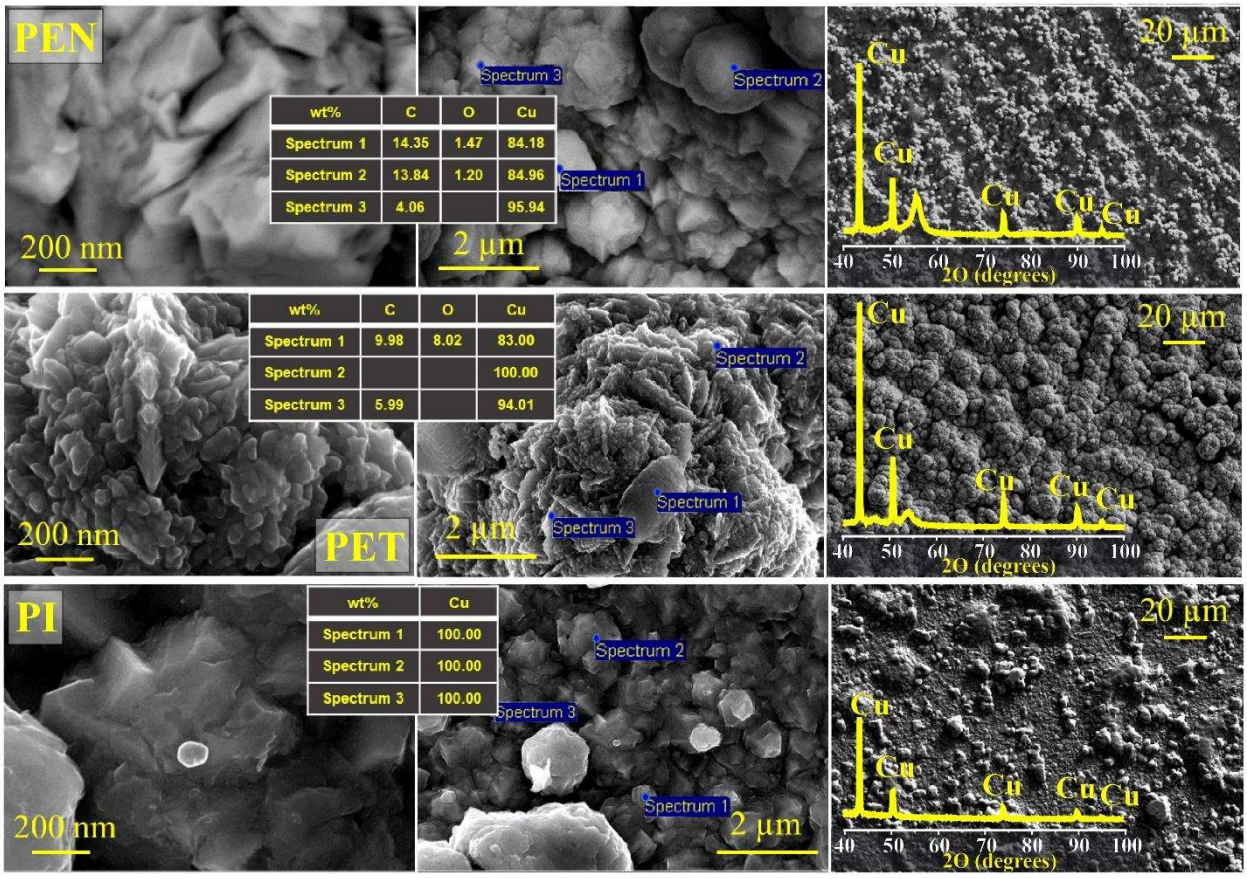

Fig. 4 SEM images, results of EDX analysis and XRD patterns of copper structures on the surface of (from top to bottom) PEN, PET and PI.

Modification of copper electrodes

To improve the analytical characteristics of the synthesized copper electrodes, we modified their surface. Modification of the electrode surface by nanomaterials can significantly improve its

sensory activity. Indeed, the electrocatalytic performance of the non-enzymatic electrode is determined not only by its nature but also by the morphology of its surface. In turn, the highest sensitivity is typical for highly porous nanostructured electrodes due to the high electrochemically active surface area. Thus, the modification and decoration of the electrodes with nanoparticles (NPs) of various shapes allows producing composite materials that can exhibit a synergistic effect leading to a significant increase in catalytic properties compared to counterparts based on individual components [55–58]. In all experiments described below, PEN was used as a substrate to demonstrate general idea of surface modification, however, proposed synthesis can be performed with PI and PET as well.

Chemical synthesis of nanostructures on the surface of copper electrode

The method of synthesis of gold NPs on the surface of copper electrode was described above. We determined the optimal conditions for the synthesis of bimetallic electrode materials based on Cu-Au. It was shown that using a component acting as a reducing agent (formaldehyde) leads to the formation of gold NPs in the entire volume of the solution. In turn, the reaction under conditions when the reduction of gold occurs due to partial dissolution of the pre-synthesized copper layer allows localizing the process on the surface of the electrode. The morphological and atomic composition studies of Cu-Au electrodes on the surface of various polymers fabricated at different conditions are presented in Figs. 5, S4-S6. It should be mentioned that the crystal Au reflexes were not found in the XRD patterns of Cu-Au electrodes (Fig. S6). It can be possibly explained by the possible formation of alloys [59] since copper tends to form them in the Cu-Au system when $HAuCl_4$ interacts with metallic copper. However, EDX mapping (Fig. 5a and S5) shows the presence of at least 2% of the mass of Au (or more, depending on the synthesis conditions) and its uniform distribution over the deposit surface. In addition, the reduction of $HAuCl_4$ and formation of Au (0) were confirmed by photoelectron spectroscopy data (Fig. 5b) [60, 61].

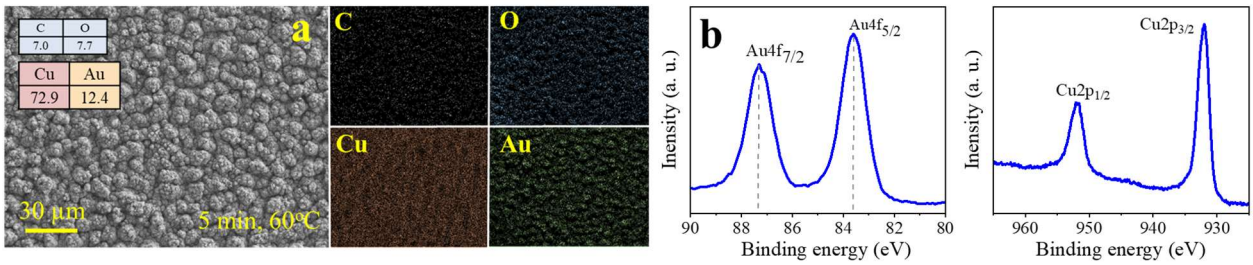

Fig. 5 (a) SEM image and EDX mapping, (b) Photoelectron spectra of bimetallic Cu-Au structures fabricated under the conditions on the surface of PEN 5 min, 60 °C

Electrochemical oxidation of the copper electrode surface

The electrode materials based on copper and gold manufactured on various polymers have metallic conductivity, which simplifies electron transfer from the electrocatalytically active surface of an electrode to the measuring circuit of a device. However, many non-metallic materials also show good electrocatalytic performance in various reactions especially in neutral media. For example, oxygen-containing copper(II) compounds reveal high activity in a number of practically important processes such as electrochemical oxidation of methanol, the splitting of water and the oxidation of glucose and dopamine [62–66].

The synthesis of oxide nanostructures on the surface of copper electrodes was described in the previous section. We estimated the influence of time of the potentiostatic synthesis (Fig. 6a) on morphology and studied the atomic composition of the formed layers (Fig. S7-S8).

The formation of hydrophilic structures with a high aspect ratio provides access of the electrolyte with the dissolved analyte to the active centers of the electrode providing an increase not only in the actual surface area but also in the electrochemical activity. EDX mapping of these electrodes showed an increase in oxygen content with an increase of the synthesis time in addition to uniform distribution of elements over the electrode surface, as well as a gradual decrease in the carbon content, the signal of which refers to PEN (Fig. S8). That may indirectly indicate an increase in the thickness of the layer of the formed oxides. Besides, it can be assumed that the phase of copper(II) oxide and copper(II) hydroxide prevails over copper(I) oxide according to the atomic composition and the ratio of Cu to O (Fig. S8).

In addition, the qualitative composition of these electrodes was determined using X-ray diffraction and Raman spectroscopy. However, the sensitivity of XRD analysis was insufficient to detect oxide phases (Fig. 6b) [67].

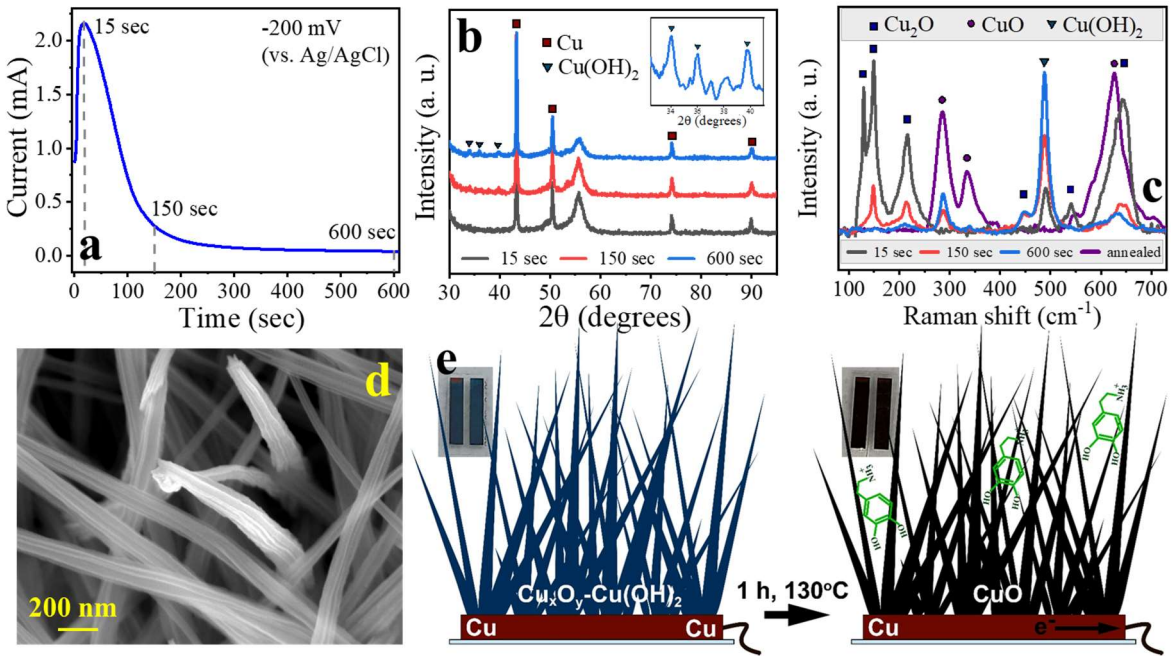

Fig. 6 (a) Amperometric curve recorded after passivation of copper deposits on the surface of PEN, (b) XRD patterns, (c) Raman scattering spectra of Cu_xO_y-$Cu(OH)_2$ nanowires on the surface of the fabricated copper electrode, (d) SEM-image of the CuO nanowires on the surface of the fabricated copper electrode after annealing, and (d) schematic illustration of the modification process.

As a result, only peaks of the initial metallic copper are presented in the X-ray diffractogram for samples obtained at a short synthesis time. $Cu(OH)_2$ reflexes begin to manifest during the prolonged passivation. At the same time, Cu_2O, CuO and $Cu(OH)_2$ signals were found in the Raman spectrum (Fig. 6c) [68–71]. Thus, the results of composition analysis do not contradict the previously proposed copper passivation mechanism in highly alkaline solutions [72]. The amperometric curve for the passivation of copper deposits on the surface of PEN is shown in Fig. 6a. Although, it has a pronounced maximum, the initial increase in the current density may indicate an increase in the surface area due to the start of active growth of the oxide layer. A further decrease in the current density is probably due to the elongation of the nanowires, which leads to an increase in the electrical resistance since the charge must pass through a growing layer of a material with

higher resistance than metallic copper [51]. After reaching the plateau, the surface morphology does not change significantly. There is a thickening of the nanowires (Fig. S7) and a redistribution of the phase composition (Fig. 6c). Moreover, SEM-image after annealing shows that the nanowires have retained their structure. Raman spectra presented in Fig. 6c confirms the formation of CuO that occurs after the annealing of the surface of electrodes (blue surface turned black, Fig. 6e).

Electrocatalytic activity of the synthesized materials

The electrocatalytic activity of the fabricated electrode materials toward D-glucose (Cu, Cu-Au electrodes), hydrogen peroxide (Cu, Cu-Au electrodes), dopamine (Cu-CuO electrodes), as well as the influence of the interfering species, were studied using cyclic voltammetry and chronoamperometry (Figs. 7 and Figs. S9-13). The CVs were recorded for different concentrations of analytes for all electrodes to determine the operating potential for further chronoamperometric measurements. Typically, the CVs of copper-based electrodes in 0.1 M NaOH have prominent anode and cathode peaks (Figs. S9a). The peaks at -0.39 (peak **1**) and -0.15 V (peak **2**) correspond to such transitions as Cu(0)/Cu(I) and Cu(0)/Cu(II) for **1** and Cu(I)/Cu(II) for **2**. A sharp increase in the current when the potential of 0.6 V is reached is due to the beginning of the electrolysis reaction of water . The Cu(II)/Cu(III) transition and formation of the catalytically active species occur at 0.5 V. Nevertheless, this peak is not pronounced, which may be due to Cu(III) species being detected only at a high concentration of hydroxide ions. A sharp increase in the anode current at 0.5 V (peak **3**) with the addition of glucose can be explained by the electrooxidation of the analyte by forming Cu(III) species. The cathode peaks correspond to the copper reduction processes (peaks **4** and **5**). In this case, a decrease in the intensity of peak **4** relating to the Cu(III)/Cu(II) transition is observed in the presence of D-glucose confirming the participation of Cu(III) in the electrocatalytic process [73, 74].

Optimal working potentials for the modified electrodes were determined. Three different potentials for each analyte were tested. Subtracting current value was used for evaluation of sensor electrocatalytic performance. This value was defined as the difference between current registered in the background solution and in presence of an analyte of 100 mM concentration [12]. Amperometric curves in 0.1 M NaOH with glucose addition was recorded at 0.35 V (vs. Ag/AgCl), 0.5 V (vs. Ag/AgCl) and 0.6 V (vs. Ag/AgCl). The corresponding calibration curves are shown in Fig. S14 a, b. The calculated value of the subtracting current indicates that optimum potential for glucose oxidation equals to 0.5 V (Fig. S14 c). The application of potential at 0.6 V provided an increase in the current within the margin of error relative to the potential of 0.5 V. Therefore, the lower potential was fixed for further experiments. Similar experiments for hydrogen peroxide and dopamine were carried out as well (Fig. S14 d,e). The optimal potentials were found to be -0.17 V (vs. Ag/AgCl) and 0.25 V (vs. Ag/AgCl) for H_2O_2 and DA, respectively.

The amperometric responses of the synthesized electrodes were measured in the background solutions with different concentrations of the target analytes (Figs. 7b, f and S9b, S10b, S11b, S12b, S13b). Thus, the calibration curves (the Faraday current vs the analyte concentration) were plotted based on these measurements (Figs. 7c,g and S9c, S10c, S11c, S12c, S13c).

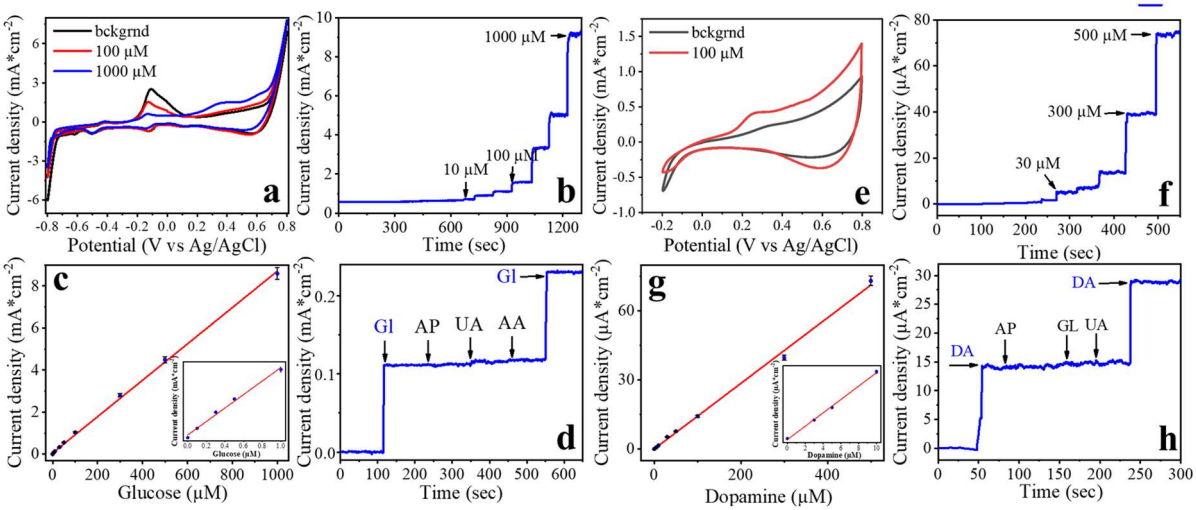

Fig. 7 Electrochemical studies of copper-gold electrode fabricated on the surface of PEN; (a) CVs measured in 0.1 M NaOH at various D-glucose concentrations; (b) Amperogram recorded in 0.1 M NaOH with different concentration of D-glucose at the potential of 0.5 V (vs Ag/AgCl); (c) Calibration plot obtained by plotting the measured Faraday current at 0.5 V (vs Ag/AgCl) as a function of D-glucose concentrations; (d) Amperometric response to successive addition of 100 µM D-glucose (Glu), 20 µM uric acid (UA), 20 µM ascorbic acid (AA) and 20 µM 4-acetamidophenol (AP) in 0.1 M NaOH. **Electrochemical studies of CuO-Cu electrode fabricated on the surface of PEN**; (e) CVs measured in 0.1 M PBS at various DA concentrations; (f) Amperogram recorded in 0.1 M PBS with different concentration of DA at the potential of 0.25 V (vs Ag/AgCl); (g) Calibration plot obtained by plotting the measured Faraday current at 0.25 V (vs Ag/AgCl) as a function of DA concentrations; (h) Amperometric response to successive addition of 100 µM DA, 100 µM uric acid (UA), 100 µM D-glucose (Gl) and 100 µM 4-acetamidophenol (AP) in 0.1 M PBS.

The selectivity of the synthesized electrodes toward enzyme-free sensing of Gl, H2O2, and DA was tested in the presence of the interfering substances, including 4-acetamidophenol (AP), ascorbic acid (AA) and uric acid (UA). These substances co-exist with the target analytes in human blood, body fluids and other potential systems of practical importance such as beverages (Figs. S9d and S10d, h). Fig. S10d illustrates the amperometric response at 0.5 V (vs. Ag/AgCl) for Cu-Au electrode in the presence of 100 µM D-glucose (Glu), 20 µM uric acid (UA), 20 µM ascorbic acid (AA) and 20 µM 4-acetamidophenol (AP) in 0.1 M NaOH. The results showed that copper-gold electrodes are highly resistant to the interfering impurities and exhibit a much higher response toward D-glucose (Fig. 7d). The selectivity towards dopamine and hydrogen peroxide was investigated as well (Figs. 7h and S9d, S10d, S11d, S12d, S13d)

Thus, it was shown that by modification of the copper electrode the surface fabricated using the method considered in this paper, it is possible to expand the basis of analytes and carry out measurements in neutral media with physiological pH. Finally, it can be concluded that the modification of copper electrodes by nanostructures significantly increases their electrochemical characteristics, along with sensitivity and limits of detection (LODs) (Table 2). The comparison of the parameters of the fabricated electrodes with those observed for recently reported analoges is presented in Tables S2-S4.

Table 2 Electrochemical parameters of the fabricated copper-based electrodes.

Electrode	Analyte	Linear range, µM	LOD*, µM	Sensitivity, µA $mM^{-1}cm^{-2}$

Cu-Au PEN	D-glucose	0.1-1000	0.05	8640
	H_2O_2	0.5-3000	0.2	2420
Cu PET	D-glucose	10-1000	2.4	1050
Cu PEN	D-glucose	3-1000	1.1	139
	H_2O_2	50-5000	20.1	139
Cu PI	D-glucose	3-1000	0.9	775
Cu-CuO PET	Dopamine	3-500	0.57	142.5

*LOD = 3σ/m, where σ is the standard deviation from linearity and m is the slope of the calibration curve shown in Figs. 14-16 and SI.

The stability tests were conducted with the modified electrodes for glucose, hydrogen peroxide and dopamine detection (Fig. S15). Background solution containing 100 μM of dopamine or glucose was used as a testing system. Five samples of each material were exploited for experiments. They exhibited appropriate levels of stability during the 21 days period, and the drop in relative current density was ~10% for all electrodes. According to the experiment design, each particular electrode (out of five sets) was used for analysis 11 times (every 2nd day for 21 days). The sample was rinsed with water, dried with air flow and stored under ambient conditions after measurement. Therefore, the results presented in Fig. S15 confirms not only stability of the electrodes, but also demonstrates the possibility of their multiple usage.

The repeatability of glucose, hydrogen peroxide and dopamine detection with the modified Cu-Au and CuO-Cu electrodes was tested by conducting 5 successive measurements in corresponding background solution containing 100 μM of analyte. Calculated relative standard deviation (RSD) equals to 2.80%, 3.51% and 3.95% for Gl, H_2O_2 and DA respectively, which shows decent repeatability of the fabricated sensors. The reproducibility of glucose, hydrogen peroxide and dopamine detection with the modified Cu-Au and CuO-Cu electrodes was tested by using 5 independent electrodes in the corresponding background solution containing 100 μM of analyte. Calculated RSD equals to 1.95%, 2.03% and 2.58% for Gl, H_2O_2 and DA, respectively, that shows decent reproducibility of the fabricated sensors.

Practical application of the fabricated Cu-Au electrodes was tested using serum samples. Amperometric experiments with serum samples diluted in 0.1 M NaOH solution were performed at the potential of 0.5 V (vs. Ag/AgCl). The results of measurements (n=3) with comparison to reference ones are presented in the Table S5. The sensor produced by SSAIL technique demonstrates decent RSD (less than 3.35%) and recovers within the range of 97.26 - 103.53 %.

In particular, bimetallic Cu-Au structures demonstrate a higher sensitivity concerning glucose analysis (more than 8 times) compared to a pure copper electrode and allow reducing LOD from 10 to 0.1 μM. On the other hand, the fabrication of the CuO layer on the surface of the copper electrode exhibits good electrocatalytic performance toward detection of dopamine at physiological conditions.

Conclusions

In this work, a promising laser-assisted technique for fabrication of sensor-active materials based on copper and other metals was proposed. In comparison with many existing analogical methods, the proposed approach does not require a template. It can be used to create metallic patterns on the surface of polymers of any desired geometry, even for small-scale production and prototyping. Typically, laser fabrication on polymer surfaces is quite difficult due to utilization of

too high laser power, at which the destruction of the substrate material may occur. Moreover, it is necessary to note that the scanning speed of the laser beam along the polymer surface may reach values of several meters per second, and the subsequent stage of chemical copper plating allows extensively increasing the amount of material fabricated per unit of time without using expensive equipment. Thus, we performed laser activation and selective copper plating of flexible polymer substrates such as PEN, PET and PI. We also produced bimetallic composites based on Cu-Au and Cu-CuO systems by modifying the previously fabricated copper structures. The electrocatalytic performance of the obtained materials toward non-enzymatic detection of such biologically important analytes as glucose, hydrogen peroxide and ascorbic acid. It was demonstrated that the modification of copper electrodes with gold-based nanostructures significantly improves their electrochemical characteristics, including sensitivity and detection limit. In turn, deposition of CuO on the surface of copper electrodes provides conditions for the dopamine acid sensing in a neutral medium. Finally, it is possible to conclude that the discussed technique can be used for synthesis and modification of electrode materials on flexible surfaces with high electrocatalytic activity toward a wide range of analytes based on a single source system. Spatially selective synthesis of other metal coatings (such as nickel, etc.) will further expand the scope of the proposed technology.

Acknowledgements
I.I.T., E.M.K. and M.S.P. acknowledge Russian Science Foundation (grant 20-79-10075).
The authors would like to thank the SPbSU Nanotechnology Interdisciplinary Centre, Centre for Physical Methods of Surface Investigation, Centre for Optical and Laser Materials Research and Centre for X-ray Diffraction Studies.

Conflicts of Interest: The authors declare no conflict of interest.

References

1. Juska VB, Pemble ME (2020) A Critical Review of Electrochemical Glucose Sensing: Evolution of Biosensor Platforms Based on Advanced Nanosystems. Sensors (Switzerland) 20:1–28. https://doi.org/10.3390/s20216013
2. Hwang DW, Lee S, Seo M, Chung TD (2018) Recent advances in electrochemical non-enzymatic glucose sensors – A review. Anal Chim Acta 1033:1–34. https://doi.org/10.1016/j.aca.2018.05.051
3. Sehit E, Altintas Z (2020) Significance of nanomaterials in electrochemical glucose sensors: An updated review (2016-2020). Biosens Bioelectron 159:112165. https://doi.org/10.1016/j.bios.2020.112165
4. Cli A, Das J, Youse H, et al (2021) Strategies for Biomolecular Analysis and Continuous Physiological Monitoring. J Am Chem Soc 143:5281−5294. https://doi.org/10.1021/jacs.0c13138
5. Jin H, Abu-raya YS, Haick H (2017) Advanced Materials for Health Monitoring with Skin-Based Wearable Devices. Adv Healthc Mater Healthc Mater 6:1700024. https://doi.org/10.1002/adhm.201700024
6. Huynh T, Haick H (2018) Autonomous Flexible Sensors for Health Monitoring. Adv Mater 30:1802337. https://doi.org/10.1002/adma.201802337
7. Zheng X, Zhang F, Wang K, et al (2021) Smart biosensors and intelligent devices for salivary biomarker detection. Trends Anal Chem 140:116281. https://doi.org/10.1016/j.trac.2021.116281

8. Yang C, Huang X, Li X, et al (2021) Wearable and Implantable Intraocular Pressure Biosensors : Recent Progress and Future Prospects. Adv Sci 8:2002971. https://doi.org/10.1002/advs.202002971
9. Koralli P, Mouzakis DE (2021) Advances in Wearable Chemosensors. Chemosensors 9:1–21. https://doi.org/10.3390/chemosensors9050099
10. Manmana Y, Kubo T, Otsuka K (2021) Recent developments of point-of-care (POC) testing platform for biomolecules. Trends Anal Chem 135:116160. https://doi.org/10.1016/j.trac.2020.116160
11. Bian S, Zhu B, Rong G, Sawan M (2021) Towards wearable and implantable continuous drug monitoring : A review. J Pharm Anal 11:1–14. https://doi.org/10.1016/j.jpha.2020.08.001
12. Yao Y, Chen J, Guo Y, et al (2021) Integration of interstitial fluid extraction and glucose detection in one device for wearable non-invasive blood glucose sensors. Biosens Bioelectron 179:113078. https://doi.org/10.1016/j.bios.2021.113078
13. Zhou X, Guo W, Yao Y, et al (2021) Flexible Nonenzymatic Glucose Sensing with One-Step Laser-Fabricated Cu2O/Cu Porous Structure. Adv Engeneering Mater 2100192. https://doi.org/10.1002/adem.202100192
14. Raymundo-Pereira PA, Gomes NO, Shimizu M, Sergio A (2021) Selective and sensitive multiplexed detection of pesticides in food samples using wearable, flexible glove-embedded non-enzymatic sensors. Chem Eng J 408:127279. https://doi.org/10.1016/j.cej.2020.127279
15. Glasscott MW, Vannoy KJ, Iresh PUA, et al (2020) Electrochemical sensors for the detection of fentanyl and its analogs : Foundations and recent advances. Trends Anal Chem 132:116037. https://doi.org/10.1016/j.trac.2020.116037
16. Liu Y, Pharr M, Salvatore GA (2017) Lab-on-Skin: A Review of Flexible and Stretchable Electronics for Wearable Health Monitoring. ACS Nano 11:9614–9635. https://doi.org/10.1021/acsnano.7b04898
17. Behrent A, Griesche C, Sippel P, Baeumner AJ (2021) Process-property correlations in laser-induced graphene electrodes for electrochemical sensing. Microchim Acta 188:159. https://doi.org/10.1007/s00604-021-04792-3
18. Zhao G, Wang X, Liu G, et al (2022) A disposable and flexible electrochemical sensor for the sensitive detection of heavy metals based on a one-step laser-induced surface modification : A new strategy for the batch fabrication of sensors. Sensors Actuators B Chem 350:130834. https://doi.org/10.1016/j.snb.2021.130834
19. Liu Y, Xue Q, Chang C, et al (2022) Highly efficient detection of Cd (II) ions by a stannum and cerium bimetal-modified laser-induced graphene electrode in water. Chem Eng J 433:133791 Contents. https://doi.org/10.1016/j.cej.2021.133791
20. Zhang Y, Li N, Xiang Y, et al (2020) A flexible non-enzymatic glucose sensor based on copper nanoparticles anchored on laser-induced graphene. Carbon N Y 156:506–513. https://doi.org/10.1016/j.carbon.2019.10.006
21. Zhao H, Su R, Teng L, et al (2022) Recent advances in flexible and wearable sensors for monitoring chemical molecules. Nanoscale 14:1653–1669. https://doi.org/10.1039/d1nr06244a
22. Kant T, Shrivas K, Dewangan K, et al (2022) Design and development of conductive nanomaterials for electrochemical sensors: a modern approach. Mater Today Chem 24:100769. https://doi.org/10.1016/j.mtchem.2021.100769
23. Zhou C, Shi N, Jiang X, et al (2022) Techniques for wearable gas sensors fabrication. Sensors Actuators B Chem 353:39–45. https://doi.org/10.1016/j.snb.2021.131133
24. Zanfrognini B, Pigani L, Zanardi C (2020) Recent advances in the direct electrochemical detection of drugs of abuse. J Solid State Electrochem 24:2603–2616. https://doi.org/10.1007/s10008-020-04686-z
25. Kant T, Shrivas K, Dewangan K, et al (2022) Design and development of conductive

nanomaterials for electrochemical sensors: a modern approach. Mater Today Chem 24:100769. https://doi.org/10.1016/j.mtchem.2021.100769
26. Camargo JR, Orzari LO, Araújo DAG, et al (2021) Development of conductive inks for electrochemical sensors and biosensors. Microchem J 164:105998 Contents. https://doi.org/10.1016/j.microc.2021.105998
27. Bariya M, Shahpar Z, Park H, et al (2018) Roll-to-Roll Gravure Printed Electrochemical Sensors for Wearable and Medical Devices. ACS Nano 12:6978–6987. https://doi.org/10.1021/acsnano.8b02505
28. Qin Y, Alam AU, Howlader MMR, et al (2016) Inkjet Printing of a Highly Loaded Palladium Ink for Integrated, Low-Cost pH Sensors. Adv Funct Mater 26:4923–493. https://doi.org/10.1002/adfm.201600657
29. Wang X, Zhang M, Zhang L, et al (2022) Inkjet-printed flexible sensors : From function materials , manufacture process , and applications perspective. Mater Today Commun 31:103263. https://doi.org/10.1016/j.mtcomm.2022.103263
30. Ambaye AD, Kefeni KK, Mishra SB, et al (2021) Recent developments in nanotechnology-based printing electrode systems for electrochemical sensors. Talanta 225:121951. https://doi.org/10.1016/j.talanta.2020.121951
31. Shin J, Jeong B, Kim J, et al (2019) Sensitive Wearable Temperature Sensor with Seamless Monolithic Integration. Adv Mater 32:1905527. https://doi.org/10.1002/adma.201905527
32. Windmiller JR, Bandodkar AJ, Valde G, et al (2012) Electrochemical sensing based on printable temporary transfer tattoos. Chem Commun 48:6794–6796. https://doi.org/10.1039/c2cc32839a
33. Cano-Raya C, Denchev ZZ, Cruz SF, Viana JC (2019) Chemistry of solid metal-based inks and pastes for printed electronics – A review. Appl Mater Today 15:416–430. https://doi.org/10.1016/j.apmt.2019.02.012
34. Panov MS, Grishankina AE, Stupin DD, et al (2020) In situ laser-induced fabrication of a ruthenium-based microelectrode for non-enzymatic dopamine sensing. Materials (Basel) 13:1–11. https://doi.org/10.3390/ma13235385
35. Shishov A, Gordeychuk D, Logunov L, et al (2021) Laser-induced deposition of copper from deep eutectic solvents: optimization of chemical and physical parameters. New J Chem 45:21896–21904. https://doi.org/10.1039/d1nj04158d
36. Smikhovskaia A V, Andrianov VS, Khairullina EM, et al (2019) Applied Surface Science In situ laser-induced synthesis of copper - silver microcomposite for enzyme-free D - glucose and L -alanine sensing. Appl Surf Sci 488:531–536. https://doi.org/10.1016/j.apsusc.2019.05.061
37. Shafeev GA, Hoffmann P (1999) Light-enhanced electroless Cu deposition on laser-treated polyimide surface. Appl Surf Sci 138–139:455–460
38. Lyalin AA, Nunuparov MS, Simakin A V, Shafeev GA (1995) Laser-assisted Etching and Metallisation of Via-Holes in Polyethylene Terephthalate. Adv Mater Opt Electron 5:299–303
39. Shafeev G, Marine W, Dallaporta H (1994) Laser assisted metallization of polyphenylquinoxaline. Thin Solid Films 241:52–56
40. Ratautas K, Andrulevičius M, Jagminienė A, et al (2019) Laser-assisted selective copper deposition on commercial PA6 by catalytic electroless plating – Process and activation mechanism. Appl Surf Sci 470:405–410. https://doi.org/10.1016/j.apsusc.2018.11.091
41. Ratautas K, Vosylius V, Jagminiene A, Stankeviciene I (2020) Laser-Induced Selective Electroless Plating on PC/ABS Polymer: Minimisation of Thermal Effects for Supreme Processing Speed. Polymers (Basel) 12:1–16. https://doi.org/10.3390/polym12102427
42. Ratautas K, Jagminienė A, Stankevičienė I, et al (2020) Evaluation and optimisation of the SSAIL method for laser-assisted selective electroless copper deposition on dielectrics. Results Phys 16:102943. https://doi.org/10.1016/j.rinp.2020.102943
43. Khairullina EM, Panov MS, Andriianov VS, et al (2021) High rate fabrication of copper

and copper-gold electrodes by laser-induced selective electroless plating for enzyme-free glucose sensing. RSC Adv 11:19521–19530. https://doi.org/10.1039/d1ra01565f
44. Kannan P, Maduraiveeran G (2022) Bimetallic Nanomaterials-Based Electrochemical Biosensor Platforms for Clinical Applications. Micromachines 13:76. https://doi.org/10.3390/mi13010076
45. Zhu H, Li L, Zhou W, et al (2016) Advances in non-enzymatic glucose sensors based on metal oxides. J Mater Chem B 4:7333. https://doi.org/10.1039/c6tb02037b
46. Wang N, Han Y, Xu Y, et al (2015) Detection of H2O2 at the Nanomolar Level by Electrode Modified with Ultrathin AuCu Nanowires. Anal Chem 87:457−463. https://doi.org/10.1021/ac502682n
47. Ngamaroonchote A, Sanguansap Y, Wutikhun T, Karn-orachai K (2020) Highly branched gold – copper nanostructures for non-enzymatic specific detection of glucose and hydrogen peroxide. Microchim Acta 187:559. https://doi.org/10.1007/s00604-020-04542-x
48. Thota S, Wang Y (2018) Colloidal Au – Cu alloy nanoparticles : synthesis , optical properties and applications. Mater Chem Front 2:1074–1089. https://doi.org/10.1039/c7qm00538e
49. Huang S, Liu L, Mei L, et al (2016) Electrochemical sensor for nitrite using a glassy carbon electrode modified with gold-copper nanochain networks. Microchim Acta 183:791–797. https://doi.org/10.1007/s00604-015-1717-z
50. Muench F, Schaefer S, Hagelüken L, et al (2017) Template-Free Electroless Plating of Gold Nanowires: Direct Surface Functionalization with Shape-Selective Nanostructures for Electrochemical Applications. ACS Appl Mater Interfaces 9:31142–31152. https://doi.org/10.1021/acsami.7b09398
51. Stepniowski WJ, Stojadinović S, Vasilić R, et al (2017) Morphology and photoluminescence of nanostructured oxides grown by copper passivation in aqueous potassium hydroxide solution. Mater Lett 198:89–92. https://doi.org/10.1016/j.matlet.2017.03.155
52. Stepniowski WJ, Misiolek WZ (2018) Review of fabrication methods, physical properties, and applications of nanostructured copper oxides formed via electrochemical oxidation. Nanomaterials 8:1–19. https://doi.org/10.3390/nano8060379
53. Li Z, Chen Y, Xin Y, Zhang Z (2015) Sensitive electrochemical nonenzymatic glucose sensing based on anodized CuO nanowires on three-dimensional porous copper foam. Sci Rep 5:1–8. https://doi.org/10.1038/srep16115
54. Mishra AK, Jarwal DK, Mukherjee B, et al (2020) Au nanoparticles modified CuO nanowireelectrode based non-enzymatic glucose detection with improved linearity. Sci Rep 10:1–10. https://doi.org/10.1038/s41598-020-67986-4
55. Wang H, Tzeng YK, Ji Y, et al (2020) Synergistic enhancement of electrocatalytic CO2 reduction to C2 oxygenates at nitrogen-doped nanodiamonds/Cu interface. Nat Nanotechnol 15:131–137. https://doi.org/10.1038/s41565-019-0603-y
56. Han Y, Wang Y, Ma T, et al (2020) Mechanistic understanding of Cu-based bimetallic catalysts. Front Chem Sci Eng 14:689–748. https://doi.org/10.1007/s11705-019-1902-4
57. Juska VB, Walcarius A, Pemble ME, et al (2019) Cu Nanodendrite Foams on Integrated Band Array Electrodes for the Nonenzymatic Detection of Glucose. ACS Appl Nano Mater 2:5878–5889. https://doi.org/10.1021/acsanm.9b01325
58. Khairullina EM, Tumkin II, Stupin DD, et al (2021) Laser-Assisted Surface Modification of Ni Microstructures with Au and Pt toward Cell Biocompatibility and High Enzyme-Free Glucose Sensing. ACS Omega 6:18099–18109. https://doi.org/10.1021/acsomega.1c01880
59. Liu Y, Hight Walker AR (2011) Preferential outward diffusion of Cu during unconventional galvanic replacement reactions between HAuCl4 and surface-limited Cu nanocrystals. ACS Nano 5:6843–6854. https://doi.org/10.1021/nn200565y
60. Radnik J, Mohr C, Claus P (2003) On the origin of binding energy shifts of core levels of supported gold nanoparticles and dependence of pretreatment and material synthesis ¨. Phys

Chem Chem Phys 5:172–177. https://doi.org/10.1039/b207290d
61. Shen L, Zhou X, Wang A (2017) Hydrothermal conversion of high-concentrated glycerol to lactic acid catalyzed by bimetallic CuAux (x =0.01-0.04) nanoparticles and their reaction kinetics. RSC Adv 7:30725–30739. https://doi.org/10.1039/C7RA04415A
62. Gizinski D, Brudzisz A, Santos JS, et al (2020) Nanostructured Anodic Copper Oxides as Catalysts in Electrochemical and Photoelectrochemical Reactions. Catalysts 10:1338. https://doi.org/10.3390/catal10111338
63. Bahrami E, Amini R, Vardak S (2021) Electrochemical detection of dopamine via pencil graphite electrodes modified by Cu/CuxO nanoparticles. J Alloys Compd 855:157292. https://doi.org/10.1016/j.jallcom.2020.157292
64. Amara U, Riaz S, Mahmood K, et al (2021) Copper oxide integrated perylene diimide self-assembled graphitic pencil for robust non-enzymatic dopamine detection. RSC Adv 11:25084–25095. https://doi.org/10.1039/d1ra03908c
65. Zheng Z, Qiu H, Zheng M, et al (2014) Selective electrochemical determination of dopamine in serum in the presence of ascorbic acid and uric acid by using a CuO nanoleaf electrode. Anal Methods 6:7923–7927. https://doi.org/10.1039/c4ay01366b
66. Fazio E, Spadaro S, Corsaro C, et al (2021) Metal-oxide based nanomaterials: Synthesis, characterization and their applications in electrical and electrochemical sensors. Sensors 21:2494. https://doi.org/10.3390/s21072494
67. Ha T, Tuyen V (2016) Phase transition of Cu2O to CuO nanocrystals by selective laser heating. Mater Sci Semicond Process 46:6–9. https://doi.org/10.1016/j.mssp.2016.01.021
68. Chen L, Zhao Y, Zhang Y, et al (2016) Design of Cu2O-Au composite microstructures for surface-enhanced Raman scattering study. Colloids Surfaces A Physicochem Eng Asp 507:96–102. https://doi.org/10.1016/j.colsurfa.2016.07.053
69. Mao Y, He J, Sun X, et al (2012) Electrochemical synthesis of hierarchical Cu2O stars with enhanced photoelectrochemical properties. Electrochim Acta 62:1–7. https://doi.org/10.1016/j.electacta.2011.10.106
70. Xu JF, Ji W, Shen ZX, et al (1999) Raman Spectra of CuO Nanocrystals. J Raman Spectrosc 30:413–415
71. Xu JF, Ji W, Shen ZX, Tang SH (1999) Preparation and Characterization of CuO Nanocrystals. J Solid State Chem 147:516–519
72. Filipic G, Cvelbar U (2012) Copper oxide nanowires: a review of growth. Nanotechnology 23:194001. https://doi.org/10.1088/0957-4484/23/19/194001
73. Gong Q, Sun L-P, Wu Z, Huo L-H (2018) Enhanced non-enzymatic glucose sensing of Cu – BTC- derived porous copper@carbon agglomerate. J Mater Sci 53:7305–7315. https://doi.org/10.1007/s10853-018-2078-x
74. Zhao J, Wang F, Yu J, Hu S (2006) Electro-oxidation of glucose at self-assembled monolayers incorporated by copper particles. Talanta 70:449–454. https://doi.org/10.1016/j.talanta.2006.03.004